



## Two dominant subseasonal variability modes of the eastern Pacific ITCZ

Xianan Jiang<sup>1,2</sup> and Duane E. Waliser<sup>1,2</sup>

Received 26 November 2008; revised 6 January 2009; accepted 26 January 2009; published 21 February 2009.

[1] Two subseasonal variability (SSV) modes over the eastern Pacific (EPAC) have been identified based on rainfall observations. The first SSV mode with a dominant period of 40 days has been documented in detail in previous studies. The second SSV mode associated with the EPAC intertropical convergence zone (ITCZ) rainfall, to the best of our knowledge, is documented for the first time, exhibiting a prevailing period of 18 days (hereafter, a 20-d SSV mode). This 20-d SSV mode is largely characterized by northward propagation. While its strongest signals are present over the EPAC, the impacts of this 20-d SSV mode are also discerned over the North American Monsoon, the Gulf of Mexico, and Caribbean Sea. Analysis of the low-frequency variability of these two SSV modes shows that they are anti-correlated on the interannual time scales. The physics responsible for the origins of the two SSV modes over the EPAC are still elusive.  
**Citation:** Jiang, X., and D. E. Waliser (2009), Two dominant subseasonal variability modes of the eastern Pacific ITCZ, *Geophys. Res. Lett.*, 36, L04704, doi:10.1029/2008GL036820.

### 1. Introduction

[2] As a dominant mode of tropical atmosphere, the subseasonal variability (SSV) with a period of 30–50 days (hereafter 40-d SSV mode) has been widely documented and found to exert significant impacts on global climate/weather systems [e.g., *Lau and Waliser, 2005; Zhang, 2005*]. This 40-d SSV mode is strongest in boreal winter, when it largely exhibits an equatorially trapped eastward propagation, and is commonly referred to as the Madden-Julian Oscillation (MJO) [*Madden and Julian, 1994*]. During boreal summer, the 40-d SSV mode exhibits prominent northward/northwestward movement over the Indian/western Pacific Oceans [e.g., *Yasunari, 1979; Hsu et al., 2004*]. This meridional propagation of the SSV is found to be closely associated with active and break phases of Asian monsoon rainfall [e.g., *Sikka and Gadgil, 1980; Waliser, 2006*].

[3] In addition to the 40-d SSV mode, a second dominant SSV mode with a prevailing period of 10–30 days (hereafter 20-d mode) has also been identified over the Asian summer monsoon sectors [e.g., *Krishnamurti and Bhalme, 1976; Chen and Chen, 1993*]. In contrast to the significant meridional migration associated with the boreal summer 40-d SSV mode, the 20-d mode generally displays a westward propa-

gation over these regions. Additionally, it has been illustrated that convective activities over the western Pacific associated with both 40-d and 20-d SSV modes can extend their remote impacts all the way to the US continent/North American Monsoon (NAM) via pronounced trans-Pacific Rossby wave-trains [e.g., *Kawamura et al., 1996; Jiang and Lau, 2008*].

[4] Meanwhile, subseasonal variations of boreal summer rainfall with two distinct time scales of 10–25 days and 25–60 days have also been illustrated over tropical and subtropical western Africa and adjacent regions of the Atlantic [e.g., *Janicot and Sultan, 2001; Sultan et al., 2003; Mounier and Janicot, 2004; Maloney and Shaman, 2008*]. The lower frequency SSV over this region is significantly correlated with global MJO activity [*Maloney and Shaman, 2008*]. While the high frequency SSV (~20-d mode) is characterized by a westward propagating signal in the convection over the Sahel latitudes [e.g., *Sultan et al., 2003; Mounier and Janicot, 2004*]. In addition, an oscillatory mode with a period of 22–28 days associated with convection over South America has also been reported [e.g., *Paegle et al., 2000*].

[5] In recent years, a similar 40-d SSV mode over the eastern Pacific (EPAC) warm pool has also attracted extensive interest, which is largely thought to be a local expression of the global circumnavigating MJO [e.g., *Maloney and Esbensen, 2007; Jiang and Waliser, 2008*]. In addition to this 40-d SSV mode, to the best of our knowledge, the high frequency SSV mode over the EPAC has not yet been well documented. As illustrated by the analysis in this paper, a second dominant subseasonal mode with a periodicity of about 18 days is indeed detected in the rainfall field over the EPAC intertropical convergence zone (ITCZ). In the following sections, temporal/spatial variability patterns associated with this high-frequency SSV mode are described and the seasonal-to-interannual variations of the activity of these two dominant SSV modes over the EPAC are also examined.

### 2. Data and Approach

[6] As given by *Jiang and Waliser [2008]*, local indices of the SSV over the EPAC are obtained by an extended empirical orthogonal function (EEOF) analysis of the TRMM (Tropical Rainfall Measuring Mission, version 3B42) rainfall over the EPAC (140°W–90°W; EQ–30°N). Before the EEOF analysis, 3-day mean rainfall data (non-overlapping) from January 1998 to December 2005 with horizontal resolution of 2 × 2 degrees are calculated based on raw TRMM dataset (0.5 × 0.5 degrees; daily), and are subject to band-pass time filtering to retain the periods of 10–90 days. The EEOF is conducted with 10 temporal lags of the 3-day mean data.

<sup>1</sup>Joint Institute for Regional Earth System Science and Engineering, University of California, Los Angeles, California, USA.

<sup>2</sup>Jet Propulsion Laboratory, California Institute of Technology, Pasadena, California, USA.

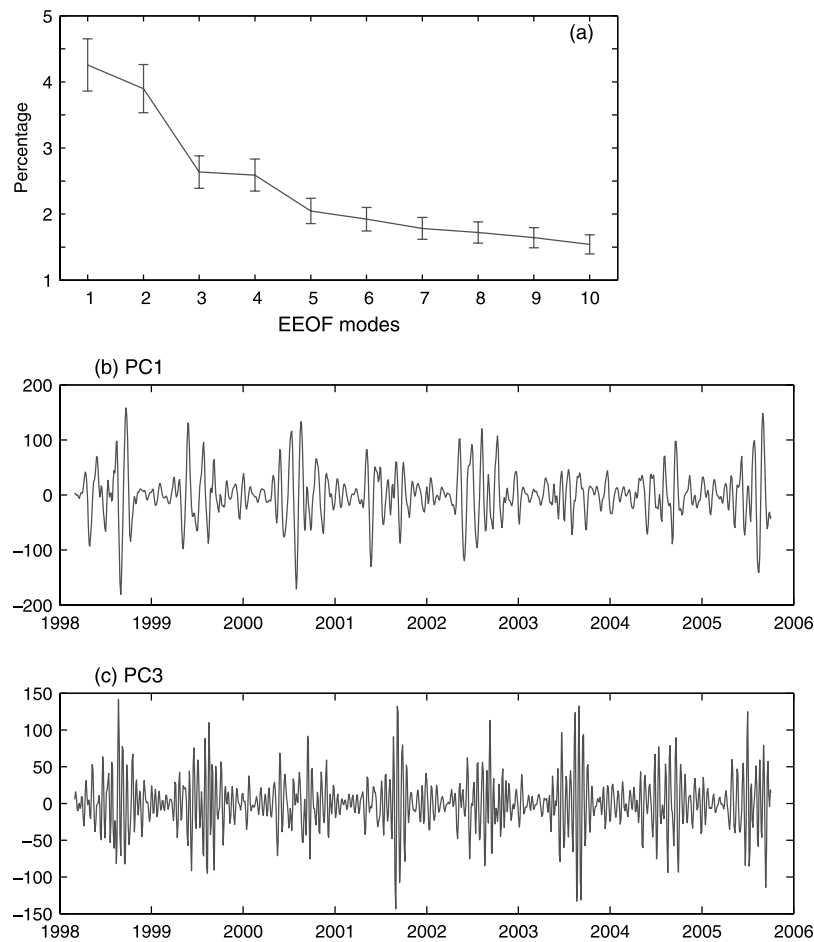


**Figure 1.** (a) EOF spectrum of TRMM rainfall over the eastern Pacific ( $140^{\circ}\text{W}$ – $90^{\circ}\text{W}$ ;  $\text{EQ}$ – $30^{\circ}\text{N}$ ) in terms of the total variance explained by each EEOF mode. Error bars are determined based on the formula by *North et al.* [1982]. Time series of temporal coefficients for the (b) EEOF<sub>1</sub> and (c) EEOF<sub>3</sub> modes.

In order to explore dynamic structures coupled with subseasonal convection signals, QuikSCAT surface wind ( $1 \times 1$  degrees; daily) during the period of 2000–2005 is also employed and subject to the same time filtering and 3-day mean bin averaging procedures as used for the TRMM rainfall.

### 3. Results

#### 3.1. Two Dominant SSV Modes Over the EPAC

[7] Figure 1a illustrates variance explained by each EEOF mode based on TRMM rainfall over the EPAC domain, where error bars are determined based on the formula by *North et al.* [1982]. It is readily seen that the first two leading pairs of the EEOF stand out from remaining EEOF modes and are also well separated from each other. The first two leading EEOFs contribute about 8.1% of total anomalous variances of band-pass filtered 3-day average data. It has been documented that the first two leading EEOFs are in quadrature to each other, and represent the same SSV mode with a period of 40 days [see *Jiang and Waliser*, 2008]. The principal components (PCs) of the EEOF<sub>1</sub> are presented in Figure 1b. This 40-d SSV mode is thought to be a local expression of the MJO signal over the

EPAC [cf. *Maloney and Esbensen*, 2007; *Jiang and Waliser*, 2008]. It is illustrated by *Jiang and Waliser* [2008] that this 40-d SSV mode over the EPAC is also characterized by a similar northward propagation as its counterpart in the Asian monsoon region. It is argued that a similar “*easterly vertical wind shear*” mechanism, which has been proposed for the meridional propagating SSV over the Indian Ocean [e.g., *Jiang et al.*, 2004], could also be dictating the northward propagation of the SSV over this region.

[8] Examination of spatial patterns and time series associated with the second pair of EEOF modes also suggests that the two modes are in quadrature to each other and exhibit similar evolution features. In contrast to 40-day period of first two leading EEOFs, both EEOF<sub>3</sub> and EEOF<sub>4</sub> display dominant periods of about 18 days (hereafter a 20-d SSV mode) based on spectral analysis of PC time series as illustrated in Figure 1c for EEOF<sub>3</sub>. This second pair of EEOFs explains about 5.1% of total variances. Comparison between Figures 1b and 1c suggests that both of the two SSV modes are active during boreal summer, while damped in winter. The interannual variability of both SSV modes can also be discerned in Figures 1b and 1c. Particularly notable is that rather weak variability of the 40-d mode in the summer of 2003. In contrast, the 20-d mode tends to be particularly

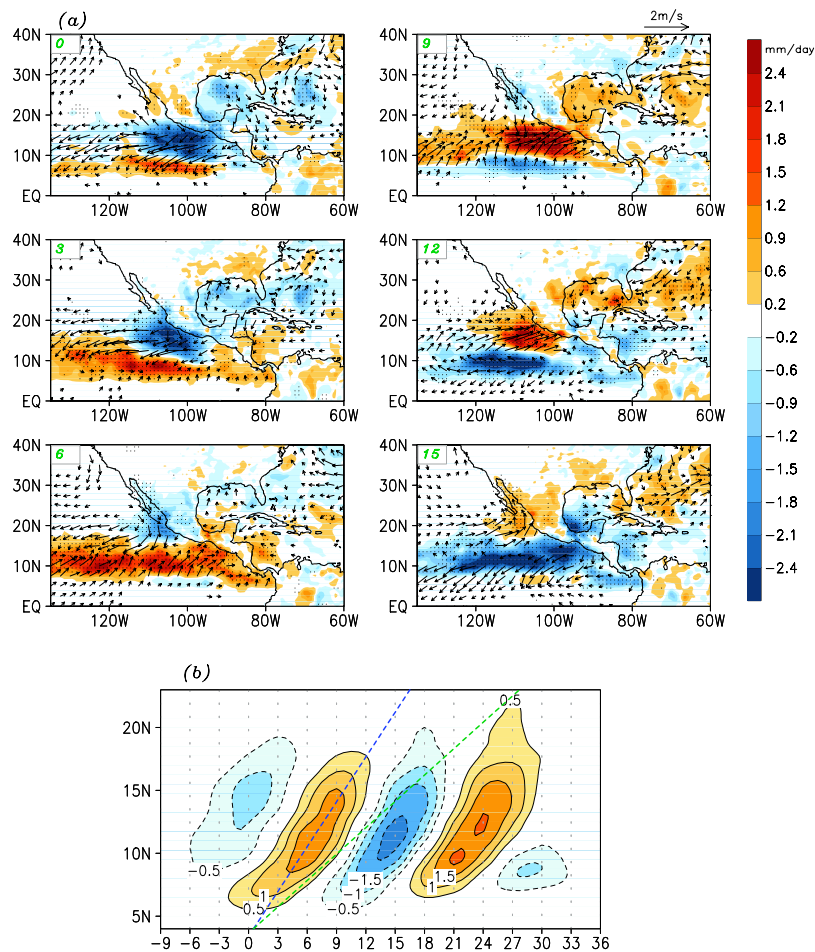


**Figure 2.** (a) Lagged regression patterns of TRMM rainfall (shaded; regions with correlation coefficients surpassing 95% significance level are stippled) and QuikSCAT surface wind (vectors) versus the standardized time series of  $PC_3$  during boreal summer (JJAS). The time interval between adjacent plots is 3 days. (b) Time-latitude distribution of rainfall perturbation averaged over the longitudes between  $130^\circ\text{W}$ – $100^\circ\text{W}$  (units:  $\text{mm day}^{-1}$ ). The dashed blue (green) line corresponds to phase speed of 1.2 (0.7)  $\text{deg day}^{-1}$ .

active during that period. This will be discussed further in the following subsection.

### 3.2. Spatial Patterns of the 20-d SSV Mode

[9] The evolution of the rainfall and wind fields over the EPAC associated with the 20-d SSV mode is illustrated in Figure 2a, which is derived by lag-regression against time series of the  $EEOF_3$ . Regions with correlation coefficients surpassing 95% significance level are stippled. (The effective degree of freedom is estimated following *Livezey and Chen* [1983], which is about 0.46 of the original sample size over the EPAC domain.) At day 0, a north-south dipole pattern in the anomalous rainfall fields (shaded) is discerned over the EPAC between  $120^\circ\text{W}$  and  $90^\circ\text{W}$ . Subsequently, the positive rainfall anomaly rapidly intensifies, and forms a zonally elongated rain band to the south of  $10^\circ\text{N}$  at day 3. In the ensuing days, both positive and negative rainfall anomalies experience northward movement with the negative anomaly weakening and dissipating near Baja California at around day 12. Meanwhile, the positive rainfall anomaly proceeds to migrate northward and is located near the Gulf of California (GoC) and part of the North America Monsoon (NAM) region at day 15. It is noted that cyclonic surface

wind flow is evident near the GoC and corresponds to the enhanced rainfall pattern. Particularly interesting is the southeasterly surface wind along the GoC, which greatly resembles the regional circulation associated with the SSV of NAM rainfall [*Jiang and Lau*, 2008], suggesting occurrence of the Gulf surge events [e.g., *Stensrud et al.*, 1997; *Higgins et al.*, 2004; *Bordoni and Stevens*, 2006]. The rainfall and wind patterns at day 15 largely mirror those at day 6, again indicating the periodicity of 18 days of this mode. Particularly noteworthy in the pattern at day 15 is that a positive rainfall anomaly begins to emerge near  $5^\circ\text{N}$ ,  $105^\circ\text{W}$  over the southeastern portion of the EPAC warm pool (also see the patterns at day 6 with an opposite sign), signifying the start of a new cycle of the oscillation as described by the patterns at day 0 and after.

[10] In addition to the EPAC and NAM region, the influence of this 20-d SSV mode can also be detected over the Gulf of Mexico (GoM), Caribbean Sea, and small portion of the North Atlantic Ocean. For instance, at day 9 when strong positive rainfall anomalies is located over the EPAC along  $15^\circ\text{N}$ , enhanced rainfall signals are noticed over the entire GoM and North Atlantic Ocean. Cyclonic circulations at the surface are also evident over these regions. After

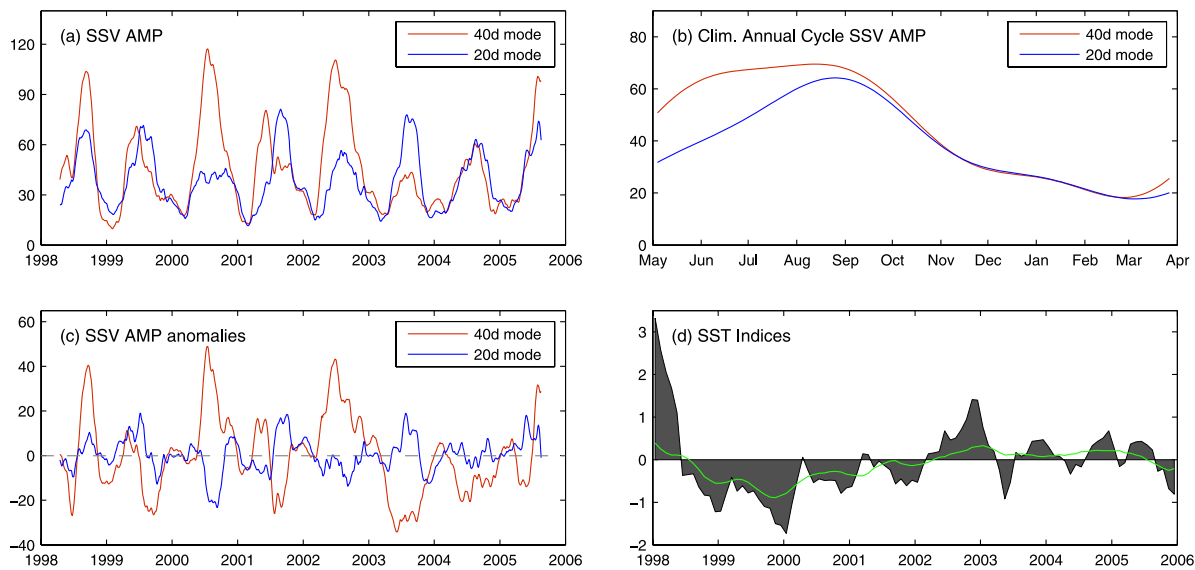


**Figure 3.** (a) The intensity of the 40-d (red curve) and 20-d (blue curve) SSV modes for the period of 1998–2005 as indicated by the combined EEOF amplitudes of  $\sqrt{PC_1^2 + PC_2^2}$  and  $\sqrt{PC_3^2 + PC_4^2}$ , respectively; (b) Climatological annual cycle (annual mean plus first three harmonics) of the intensity of the two SSV modes; (c) Same as in (a), except that the climatological annual cycle has been removed for each mode; (d) Time series of monthly Nino3 SST (adopted from website <http://www.cpc.ncep.noaa.gov/data/indices/sstoi.indices>; dark shading), and SST anomalies over the EPAC ( $130^\circ\text{W}$ – $90^\circ\text{W}$ ,  $5^\circ\text{N}$ – $20^\circ\text{N}$ ; green curve) based on NOAA OI SST V2 (units: K).

the positive rain band over the EPAC propagates to the north and suppressed rainfall anomalies become dominant over the EPAC along  $10^\circ\text{N}$  at day 15, the western part of the GoM and Caribbean Sea off the coast of Mexico/central America are characterized by suppressed rainfall.

[11] It has been illustrated that the 20-d SSV mode over the Asian and African monsoon regions is mainly characterized by pronounced westward propagation. However, as shown above, the 20-d SSV mode over the EPAC largely exhibits meridional migration. A Hovmöller diagram of rainfall over the longitudes of  $130^\circ\text{W}$ – $100^\circ\text{W}$  is displayed in Figure 2b. The northward propagation with a phase speed about  $1.2 \text{ deg day}^{-1}$  is readily evident associated with the 20-d SSV mode, much faster than that of the 40-d mode over this region ( $\sim 0.7 \text{ deg day}^{-1}$  [Jiang and Waliser, 2008]).

### 3.3. Interannual Variations in Activities of the Two SSV Modes

[12] Interannual variations of intensity of the two SSV modes from 1998–2005 are displayed in Figure 3a. The activity of the 40-d (20-d) SSV mode is defined by the combined amplitudes of the PCs of EEOF<sub>1</sub> and EEOF<sub>2</sub> (EEOF<sub>3</sub> and EEOF<sub>4</sub>), and is subject to 90-day running mean. The interannual variations in the intensity of both SSV modes are readily evident. Particularly interesting to note is the anti-correlated relationship in the intensity of these two modes. For instance, in summers when the 40-d mode is active (e.g., 2000, 2002), the intensity of 20-d mode is relatively weak. On the contrary, as discussed above, when the intensity of the 20-d mode is strong during summer of 2003, the 40-d mode is extremely weak. It is also noticed that the 40-d mode is active during early summer of 2001 when the 20-d is weak; while in later summer of this year, the 20-d mode becomes dominant relative to the 40-d mode. The anti-correlation between the 40-d and 20-d modes is more clearly

evident in Figure 3c particularly during years from 2000–2004, where the climatological annual cycles of the SSV intensity (Figure 3b) for both modes are removed from Figure 3a. Although the absence of clear anti-correlation is also seen during brief periods (e.g., in 1998), the correlation coefficient between these two time series during eight summer seasons (June–September) is about  $-0.48$  based on monthly mean data, surpassing the 96% significance level based on 10000 realizations of Monte Carlo simulation procedures [e.g., Livezey and Chen, 1983]. This anti-correlation between the 40-d and 20-d SSV modes over the EPAC largely resembles that reported over the South China Sea region [Kajikawa and Yasunari, 2005; Yang et al., 2008].

[13] To further explore the potential impacts of the sea surface temperature (SST) on the variability of the two SSV modes, time series of the Nino3 (dark shading) SST index and SST anomalies over the EPAC warm pool ( $130^\circ\text{W}$ – $90^\circ\text{W}$ ;  $5^\circ\text{N}$ – $20^\circ\text{N}$ ; green curve) are displayed in Figure 3d. The correlations between the two SST indices and SSV activities during summertime are rather weak. These results generally indicate that the El Niño or the local SST over the EPAC warm pool may not be the determining factor in controlling the interannual variability of the two SSV modes over the EPAC.

## 4. Summary and Discussion

[14] Based on an EEOF analysis of the TRMM rainfall over the EPAC during eight years period, two dominant SSV modes are identified by two well-separated leading pairs of EEOFs. The first SSV mode with a dominant period of 40 days has been documented in detail by previous studies. This 40-d SSV mode largely exhibits an eastward propagation over the EPAC although a northward movement component is also noted [Jiang and Waliser, 2008]. The

second SSV mode associated with the eastern Pacific ITCZ rainfall, which is documented for the first time to the best of our knowledge, displays a prevailing period of 18 days (e.g., a 20-d SSV mode). While its strongest signals are present over the eastern Pacific, the influence of this 20-d SSV mode could also be found over the NAM region, the GoM, Caribbean Sea, and other neighboring areas.

[15] It is noted that 20-day SSV signals associated with regional climate over Southwestern U.S. have been reported by many previous studies [e.g., Mullen *et al.*, 1998; Mo, 2000; Kiladis and Hall-McKim, 2004; Mo and Nogues-Paegle, 2005; Jiang and Lau, 2008]. In particular, Jiang and Lau [2008] illustrate similar features of the Gulf surge activities over the GoC associated with the NAM rainfall over Arizona/New Mexico region (AZNM; 32–36°N; 112–107°W) as discussed in Figure 2a. However, analysis indicates a weak correlation between the 20-d SSV mode described in this study and the AZNM rainfall index (correlation coefficients during JJAS are less than 0.13 at all time lags). Meanwhile, a pronounced trans-Pacific teleconnection wave-train associated with the AZNM rainfall as suggested by Jiang and Lau [2008] are not clearly evident in the regression patterns based on the 20-d mode of the EPAC ITCZ. Moreover, the 20-d SSV mode in the present study exhibits its strongest intensity in late August/early September as indicated by the climatological annual cycle of variability (Figure 3b). In contrast, the AZNM rainfall generally exhibits strong activities in early July associated with the NAM onset over this region (figure not shown). Whether these 20-d SSV signals over the Southwestern U.S. as reported in the previous studies are independent from the 20-d SSV mode of the EPAC ITCZ as described in the present study, or they are just local manifestation of a same SSV mode, warrants further investigation.

[16] In contrast to the 20-d SSV over the Asian monsoon sectors, which is characterized by a pronounced westward movement, the 20-d SSV mode over the EPAC largely exhibits a northward propagating component with a phase speed of about  $1.2 \text{ deg day}^{-1}$ . This meridional propagation speed is much faster than that of the 40-d mode over this region ( $\sim 0.7 \text{ deg day}^{-1}$ ). It is also noted that the initiation of the 40-d SSV mode tends to begin over the southwestern portion of the EPAC warm pool around 130°W, 8°N [see Jiang and Waliser, 2008, Figure 2]. In contrast, the 20-d SSV mode tends to reinitiate over the southeastern part of the EPAC (100°W, 5°N). The distinct initiation behaviors of these two SSV modes may suggest different origins of them. As indicated by previous studies, the 40-d mode could be associated with the circumnavigating MJO signals from the west; while, the 20-d SSV mode could be a local oscillation as seems to be the case over the aforementioned Asian summer regions. Further work is needed to understand the mechanisms of this mode, and our model and forecast capability of describing this variability and its impacts on weather/climate.

[17] Further analysis indicates that the activities of the two SSV modes over the EPAC are anti-correlated on seasonal-to-interannual time scales. A similar feature has been suggested for the SSV over the South China Sea (SCS) during June–July [Kajikawa and Yasunari, 2005; Yang *et al.*, 2008]. Yang *et al.* [2008] indicated that the 12–25-day SSV mode over the SCS is largely associated with Rossby-

wave emanation over the western Pacific, which could be tightly linked to the easterly vertical wind shear; while the 30–50-day SSV mode is associated with mean convective condition over the eastern Indian Ocean. Since these two large-scale conditions occur in isolation, the activities of the two SSV modes over the SCS tend to be anti-correlated. The physics responsible for the anti-correlation of the two modes over the EPAC is still not clear, and represents a topic for the future study.

[18] It is noteworthy that a similar EEOF analysis for the NOAA outgoing longwave radiation (OLR) over the EPAC domain has also been conducted as for the TRMM rainfall. The result indicates that the 20-d SSV mode as described above does not stand out as a well-separated leading mode based on the OLR analysis. In the future study, we will also investigate the identification of these modes with other variables, including dynamical fields, and possibly based on a combined EOF approach.

[19] **Acknowledgments.** The TRMM 3B42 rainfall dataset was processed and provided by B. Tian. We also thank G. Kiladis and anonymous reviewers for their insightful comments on an earlier version of this manuscript. The research described in this paper carried out at the Jet Propulsion Laboratory, California Institute of Technology, was done so under a contract with the National Aeronautics and Space Administration.

## References

- Bordoni, S., and B. Stevens (2006), Principal component analysis of the summertime winds over the Gulf of California: A gulf surge index, *Mon. Weather Rev.*, *134*, 3395–3414.
- Chen, T. C., and J. M. Chen (1993), The 10–20-day mode of the 1979 Indian monsoon—Its relation with the time-variation of monsoon rainfall, *Mon. Weather Rev.*, *121*, 2465–2482.
- Higgins, R. W., W. Shi, and C. Hain (2004), Relationships between Gulf of California moisture surges and precipitation in the southwestern United States, *J. Clim.*, *17*, 2983–2997.
- Hsu, H. H., C. H. Weng, and C. H. Wu (2004), Contrasting characteristics between the northward and eastward propagation of the intraseasonal oscillation during the boreal summer, *J. Clim.*, *17*, 727–743.
- Janicot, S., and B. Sultan (2001), Intra-seasonal modulation of convection in the West African monsoon, *Geophys. Res. Lett.*, *28*, 523–526.
- Jiang, X., and N.-C. Lau (2008), Intraseasonal teleconnection between North American and western North Pacific monsoons with 20-day time scale, *J. Clim.*, *21*, 2664–2679.
- Jiang, X., and D. E. Waliser (2008), Northward propagation of the subseasonal variability over the eastern Pacific warm pool, *Geophys. Res. Lett.*, *35*, L09814, doi:10.1029/2008GL033723.
- Jiang, X., T. Li, and B. Wang (2004), Structures and mechanisms of the northward propagating boreal summer intraseasonal oscillation, *J. Clim.*, *17*, 1022–1039.
- Kajikawa, Y., and T. Yasunari (2005), Interannual variability of the 10–25- and 30–60-day variation over the South China Sea during boreal summer, *Geophys. Res. Lett.*, *32*, L04710, doi:10.1029/2004GL021836.
- Kawamura, R., T. Murakami, and B. Wang (1996), Tropical and mid-latitude 45-day perturbations over the western Pacific during the northern summer, *J. Meteorol. Soc. Jpn.*, *74*, 867–890.
- Kiladis, G. N., and E. A. Hall-McKim (2004), Intraseasonal modulation of precipitation over the North American monsoon region, paper presented at the 15th Symposium on Global Change and Climate Variations, Am. Meteorol. Soc., Seattle, Wash.
- Krishnamurti, T. N., and H. N. Bhalme (1976), Oscillations of a monsoon system: 1. Observational aspects, *J. Atmos. Sci.*, *33*, 1937–1954.
- Lau, W. K.-M., and D. E. Waliser (2005), *Intraseasonal Variability in the Atmosphere-Ocean Climate System*, 474 pp., Springer, Heidelberg, Germany.
- Livezey, R. E., and W. Y. Chen (1983), Statistical field significance and its determination by Monte-Carlo techniques, *Mon. Weather Rev.*, *111*, 46–59.
- Madden, R. A., and P. R. Julian (1994), Observations of the 40–50-day tropical oscillation: A review, *Mon. Weather Rev.*, *122*, 814–837.
- Maloney, E. D., and S. K. Esbensen (2007), Satellite and buoy observations of boreal summer intraseasonal variability in the tropical northeast Pacific, *Mon. Weather Rev.*, *135*, 3–19.
- Maloney, E. D., and J. Shaman (2008), Intraseasonal variability of the West African monsoon and Atlantic ITCZ, *J. Clim.*, *21*, 2898–2918.

- Mo, K. C. (2000), Intraseasonal modulation of summer precipitation over North America, *Mon. Weather Rev.*, *128*, 1490–1505.
- Mo, K. C., and J. Nogués-Paegle (2005), Pan-America, in *Intraseasonal Variability in the Atmosphere-Ocean Climate System*, edited by W. K. M. Lau and D. E. Waliser, pp. 389–424, Springer, Heidelberg, Germany.
- Mounier, F., and S. Janicot (2004), Evidence of two independent modes of convection at intraseasonal timescale in the West African summer monsoon, *Geophys. Res. Lett.*, *31*, L16116, doi:10.1029/2004GL020665.
- Mullen, S. L., J. T. Schmitz, and N. O. Rennó (1998), Intraseasonal variability of the summer monsoon over southeast Arizona, *Mon. Weather Rev.*, *126*, 3016–3035.
- North, G. R., T. L. Bell, R. F. Cahalan, and F. J. Moeng (1982), Sampling errors in the estimation of empirical orthogonal functions, *Mon. Weather Rev.*, *110*, 699–706.
- Paegle, J. N., L. A. Byerle, and K. C. Mo (2000), Intraseasonal modulation of South American summer precipitation, *Mon. Weather Rev.*, *128*, 837–850.
- Sikka, D. R., and S. Gadgil (1980), On the maximum cloud zone and the ITCZ over Indian, longitudes during the southwest monsoon, *Mon. Weather Rev.*, *108*, 1840–1853.
- Stensrud, D. J., R. L. Gall, and M. K. Nordquist (1997), Surges over the Gulf of California during the Mexican monsoon, *Mon. Weather Rev.*, *125*, 417–437.
- Sultan, B., S. Janicot, and A. Diedhiou (2003), The West African monsoon dynamics. Part I: Documentation of intraseasonal variability, *J. Clim.*, *16*, 3389–3406.
- Waliser, D. E. (2006), Intraseasonal variations, in *The Asian Monsoon*, edited by B. Wang, p. 787, Springer, Heidelberg, Germany.
- Yang, J., B. Wang, and B. Wang (2008), Anticorrelated intensity change of the quasi-biweekly and 30–50-day oscillations over the South China Sea, *Geophys. Res. Lett.*, *35*, L16702, doi:10.1029/2008GL034449.
- Yasunari, T. (1979), Cloudiness fluctuations associated with the Northern Hemisphere summer monsoon, *J. Meteorol. Soc. Jpn.*, *57*, 227–242.
- Zhang, C. (2005), Madden-Julian Oscillation, *Rev. Geophys.*, *43*, RG2003, doi:10.1029/2004RG000158.

---

X. Jiang and D. E. Waliser, Jet Propulsion Laboratory, California Institute of Technology, 4800 Oak Grove Dr., Pasadena, CA 91109, USA. (xianan@jifresse.ucla.edu)